Petroleum Science 23 (2026) 5757–5769

Contents lists available at ScienceDirect

Petroleum Science

journal homepage: www.keaipublishing.com/en/journals/petroleum-science

Original Paper

Thermally activated self-adhesive flexible granules for sealing fractures in high-temperature and high-salinity reservoirs: Synthesis, tunability, and performance evaluation

Yan Xue [a,*], Xiao-Feng Zhao [a], Qiu-Lu Yin [a], Jing-Yang Gu [a], Bing Wei [b,**], Jun Lu [c]

[a] Oil & Gas Field Applied Chemistry Key Laboratory of Sichuan Province, College of Chemistry and Chemical Engineering, Southwest Petroleum University, Chengdu, 610500, Sichuan, China
[b] State Key Laboratory of Oil and Gas Reservoir Geology and Exploitation, Southwest Petroleum University, Chengdu, 610500, Sichuan, China
[c] McDougall School of Petroleum Engineering, The University of Tulsa, Tulsa, OK 74101, USA

A R T I C L E I N F O

Article history:
Received 5 February 2026
Received in revised form
8 June 2026
Accepted 9 June 2026
Available online 13 June 2026

Edited by Yan-Hua Sun

Keywords:
Fracture sealing
Self-adhesion
Response surface methodology
High-temperature and high-salinity reservoir

A B S T R A C T

To overcome the limitations of conventional preformed particle gels in ultra-high-temperature and high-salinity fractured reservoirs, this study developed a novel self-adhesive flexible granule (SAFG). SAFG is synthesized through a two-step process involving the hydrophobic modification of polyvinyl alcohol, followed by chemical cross-linking with terephthalaldehyde, resulting in a stable granular structure. Comprehensive characterization confirmed the successful synthesis, tunable granule size controlled by stirring speed, and exceptional long-term thermal stability in high-salinity brine (2.1×10^5 mg/L, 130 °C for 180 d). Response surface methodology (RSM) optimization determined the optimal synthesis parameters, yielding granules with superior comprehensive performance. SAFG exhibits a unique, tunable self-adhesion mechanism activated by elevated temperature in high-salinity brine, transforming into a cohesive bulk gel. Core-flooding experiments demonstrated effective migration and dynamic plugging in simulated fractures (fracture widths of 0.5 and 1.0 mm), with optimal performance observed at injection rates of 1.5–2.5 mL/min and SAFG concentrations of 5.0 wt%. Critically, after thermally assisted adhesion aging, the adhered SAFG structure achieved a breakthrough pressure of 3080 kPa, approximately 6.3 times the initial stabilization pressure, confirming its robust sealing capability. This work demonstrates SAFG as a robust and tunable conformance control agent for extreme reservoir conditions, offering a viable solution to enhance oil recovery in challenging fractured formations.

1. Introduction

The advancement of oilfield development into high-water-cut stages presents a significant challenge to sustainable hydrocarbon recovery. Long-term waterflooding operations, while essential for pressure maintenance, often exacerbate reservoir heterogeneity by promoting the formation of dominant flow pathways such as fractures, high-permeability channels, and vuggy conduits (Salunkhe et al., 2021; Seright and Brattekas, 2021). These features facilitate severe water channeling, leading to a rapid decline in oil production and a substantial increase in water production and associated management costs. It is estimated that the global oil industry spends approximately USD 40–55 billion annually on managing produced water, with the average water–oil ratio exceeding 3:1 and reaching as high as 7:1 in some mature fields (Kumar et al., 2020; Leng et al., 2021). When the economic burden of water handling surpasses the value of the produced oil, premature well abandonment becomes inevitable (Xue et al., 2024). Consequently, developing effective conformance control technologies to plug these large flow paths and redirect injected fluids is critical for enhancing volumetric sweep efficiency and extending the economic life of heterogeneous and fractured reservoirs (Wu et al., 2023).

* Corresponding author.
** Corresponding author.
E-mail addresses: yxue@swpu.edu.cn (Y. Xue), bwei@swpu.edu.cn (B. Wei).
Peer review under the responsibility of China University of Petroleum (Beijing).

https://doi.org/10.1016/j.petsci.2026.06.019
1995-8226/

Traditional in-situ gel systems, though widely studied, face inherent operational and performance limitations (Seidy Esfahlan et al., 2021). These include difficulties in controlling gelation time, chromatographic fractionation of gelants during propagation through heterogeneous media, shear degradation during injection, and the potential for damaging low-permeability, oil-bearing zones (Gao et al., 2026). To overcome these issues, preformed particle gels (PPGs) were developed. PPGs offer improved operational controllability and significantly reduce the risk of formation damage (Qiu et al., 2017; Sun et al., 2020; Wang and Bai, 2018). However, conventional PPGs, typically based on polyacrylamide chemistries, often lack sufficient mechanical elasticity, long-term thermal stability, and inherent adhesion properties (Bai et al., 2015; Zhang et al., 2022b). Under the extreme conditions of high-temperature and high-salinity reservoirs, they struggle to effectively seal large fracture apertures or vuggy spaces (Mehrabianfar et al., 2020; Schuman et al., 2022). Their plugging efficiency in macro-scale conduits is further compromised by inadequate particle–particle and particle–rock adhesion, often resulting in washout after water breakthrough (Bu et al., 2024; Wang et al., 2017).

Recent research has focused on enhancing PPG technology through the development of recrosslinkable PPGs (RPPGs). These materials aim to combine the advantages of in-situ crosslinking with the controllability of conventional PPGs (Al Brahim et al., 2023; Zhai et al., 2024). RPPGs are designed to undergo shape-adaptive re-cohesion within high-permeability fractures, enabling particle integration into a cohesive mass for deep-profile water plugging (Alotibi et al., 2025; Pu et al., 2019). To enhance the application performance of RPPG, Wang et al. (2017) fabricated a high-strength RPPG with re-crosslinking capability through reversible ionic crosslinking of brine-induced preformed particle gels. Song et al. (2022) conducted a comprehensive laboratory evaluation of HT-BRPPG, a novel hyperbranched RPPGs designed for North Sea high-temperature sandstone reservoirs, which can re-crosslink into rubbery bulk gels for reservoir plugging, with the re-crosslinked gel achieving an elastic modulus of 830 Pa. Zhao et al. (2022) demonstrated fiber-assisted RPPGs in fracture models, revealing fiber entanglement effects on gel quality and plugging efficiency. While these advancements underscore the significant potential of particle-based systems, they simultaneously highlight a persistent gap: the need for a material that possesses superior long-term stability, robust self-adhesion capability, and adequate deformation capacity under the most extreme reservoir conditions.

The fracture-vuggy carbonate reservoirs exemplified by China's Tarim Basin (e.g., Tahe Oilfield) exhibit extreme conditions: temperatures of 120–140 °C, high pressures (54–88 MPa), and salinities exceeding 2.1×10^5 mg/L (Wu et al., 2022). These harsh environments challenge waterflooding efficiency and oil recovery. While RPPGs represent a step forward, there remains a clear and pressing need for a more robust conformance control agent. The ideal material must not only withstand ultra-high temperature, high pressure, and high salinity but also reliably plug large fracture channels through mechanisms that ensure stable, durable aggregation and adhesion within the target zone. To address these critical challenges, this study introduces a novel self-adhesive flexible granule (SAFG) system, specifically engineered for conformance control in fractured, high-salinity reservoirs. The SAFGs are synthesized from polyvinyl alcohol (PVA) through a sequential process involving hydrophobic modification followed by chemical cross-linking with terephthalaldehyde (TAD). This molecular design intentionally incorporates rigid aromatic structures from the TAD cross-linker, which are hypothesized to significantly enhance the network's thermal resistance and mechanical strength under harsh downhole conditions. Furthermore, the granules are produced in a single-pot process with easily tunable granule sizes, offering manufacturing simplicity and the flexibility to match specific fracture apertures. Moving beyond the conventional PPG mechanisms that rely primarily on swelling and mechanical trapping, the SAFG integrates an inherent and tunable adhesion capability coupled with thermoplastic behavior. This unique combination allows the granules to undergo thermally assisted aggregation, surface adhesion, and plastic deformation under reservoir conditions. This facilitates deep migration into fracture networks and, upon thermal activation, the formation of a cohesive, durable bulk seal through granule self-adhesion and fusion.

In this work, we detail the design rationale, optimized synthesis, and comprehensive performance evaluation of the SAFGs, with particular emphasis on its unique salinity-dependent and thermally activated self-adhesion mechanism, its exceptional long-term stability under extreme conditions (up to 130 °C and 2.1×10^5 mg/L salinity), and its systematic migration and dynamic plugging behavior in simulated fracture models. The development of SAFG provides a new material strategy for conformance control in the most challenging reservoirs where traditional gels and existing PPGs exhibit limited effectiveness, offering a promising pathway to improve oil recovery and sustainably manage water production in highly heterogeneous, fractured formations under extreme downhole conditions.

2. Experimental section

2.1. Materials

Polyvinyl alcohol 1799 (PVA-1799) and terephthalaldehyde (TAD, 99% purity) were obtained from Macklin Biochemical Technology Co., Ltd. (Shanghai, China). Partially hydrolyzed polyacrylamide (HPAM) with a molecular weight of 1.4×10^7 g/mol and a degree of hydrolysis of 13% was supplied by Condice Chemical Co., Ltd. (Hubei, China). A hydrophobic modifier (HA) featuring a propyl group was synthesized in the laboratory. Synthetic brine was prepared based on the composition of formation water from the Tahe Oilfield, which has a total salinity of approximately 2.1×10^5 mg/L, including high concentrations of divalent cations (1.2×10^4 mg/L of Ca^{2+} and Mg^{2+}, see Table S1).

2.2. Preparation of self-adhesive flexible granule (SAFG)

PVA (7.5 g) was dissolved in deionized water (92.5 g) under stirring at 95 °C for 2 h. Dilute hydrochloric acid (6 mol/L) was then added, and the mixture was cooled to 20 °C. HA (1.6 g) was added dropwise, followed by continuous stirring for 1 h, during which metastable gel particles with a granular structure were formed. The system was then allowed to react sequentially at 25 °C for 1 h and 30 °C for 1 h each. Finally, at 40 °C, an appropriate amount of TAD (0.014 g) was introduced, and the reaction was continued for another hour. Throughout the process, SAFGs gradually precipitated in a granular form without any agglomeration.

2.3. Characterization

The chemical structures of PVA and SAFGs were analyzed by Fourier-transform infrared (FT-IR) spectroscopy (Nicolet 10, Thermo Fisher Scientific, USA) using KBr pellets over the range of 4000–400 cm^{-1} at a resolution of 4 cm^{-1}. The microstructure was examined using scanning electron microscopy (SEM; SU8010, Hitachi, Japan) at 20.0 kV after gold sputtering of freeze-dried samples. Thermal decomposition behavior was evaluated via thermogravimetric analysis (TGA; STA6000, Mettler Toledo, Switzerland) under a nitrogen atmosphere from 40 to 600 °C at a heating rate of 10 °C/min. The thermally activated adhesion temperatures of SAFGs with different modification degrees were determined using differential scanning calorimetry (DSC; Q20, TA Instruments, USA) over a temperature range of 40 to 150 °C with a heating rate of 10 °C/min.

2.4. Effect of stirring speed on granule size

Gel granules were prepared under different stirring speeds (280, 310, 340, and 370 rpm). The granule size distribution was determined by sieving, and the mass percentage of granules in each size range was calculated. The relationship between granule size and stirring speed was analyzed.

2.5. Mechanical characterization

The mechanical properties of SAFGs were characterized by their compressibility. Flexible granules undergo deformation under compression, leading to a reduction in elastic volume. In this study, the compressibility of flexible granules was tested using a custom-made mold (Fig. S1) and a universal testing machine (INSTRON 5982, INSTRON, USA). The specific test procedure was as follows: 3 g of SAFGs were placed into the groove of the custom-made mold, and the mold was repeatedly tapped to achieve dense packing. The mold cap was then securely fastened, and the initial height (H_0) of the samples was recorded. The entire assembly was positioned on the testing platform of a universal testing machine. The compression probe was lowered at a constant speed of 5 mm/s until the granules were fully compressed, and the compressed height (H_c) was recorded. The compression ratio of the granules was calculated based on these measurements ($K_c = H_c/H_0$). A lower K_c value indicates higher compressibility, which is desirable for granules to deform and adapt within fractures.

2.6. Synthesis optimization by response surface methodology (RSM)

An integrative method of Box–Behnken (BBD) (Tak et al., 2015) and RSM was employed to optimize the synthesis conditions of SAFGs. Prior to the response surface experiments, single-factor tests were conducted to determine the approximate ranges of stirring speed, modifying agent HA content, and PVA solution concentration that could yield well-formed flexible granules. Using Design Expert 13 software, a Box–Behnken Design (BBD) was adopted to plan the experimental scheme. Three independent variables were chosen, mechanical stirring speed (X_1), hydrophobic modifying agent content (X_2), and PVA solution concentration (X_3). The response was the comprehensive score evaluating particle distribution, mechanical properties, swelling behavior, and temperature/salt resistance. A total of 17 experimental runs were designed. The factors and their coded levels are presented in Table 1. The optimal predictor quadratic model presented in Eq. (1) (Auta and Hameed, 2011):

$$Y = \beta_0 + \sum_{i=1}^{k}\beta_i X_i + \sum_{i=1}^{k}\beta_{ii} X_i^2 + \sum_{j=2}^{k}\sum_{i=1}^{j=1}\beta_{ij} X_i X_j \tag{1}$$

where Y is the predicted response; β_0, β_i, β_{ii}, and β_{ij} are regression coefficients of factors X_i and X_j of independent variables; and k is the number of factors.

As this work involved a multi-objective optimization, a comprehensive scoring system was implemented to evaluate the performance of each experimental run. Following the 17 response surface experiments, the SAFGs from each group were assessed based on four key criteria: yield, swelling degree, thermal stability, and mechanical properties. Each criterion was scored according to predefined rules, and the weighted scores were summed to produce a total composite score, enabling a systematic analysis of the effects of the independent variables. The scoring weightings were designed to align with practical application requirements, wherein the primary mechanism of the synthesized flexible particles is high-temperature adhesion and sealing, with volumetric filling being a secondary function. Consequently, swelling degree and mechanical properties were assigned comparatively lower weights, as only a minimum threshold of compressive performance is necessary. The detailed scoring rubric is provided in Table 2. The optimization objective was to identify synthesis conditions that maximize the composite score while ensuring each individual response remains within its acceptable target range.

Table 1
Levels of independent variables designed in RSM.

Variable	Unit	Code	Levels		
			−1	0	1
Stirring speed	rpm	X_1	310	340	370
m(HA/PVA)[a]	wt%	X_2	20.0	21.5	23.0
c(PVA)[b]	wt%	X_3	6.0	7.5	9.0

[a] Mass content of HA relative to PVA.
[b] PVA solution concentration.

2.7. Effect of hydrophobic modification on self-adhesion temperature

The dosage of the hydrophobic modifier (HA) was varied to achieve mass percentages of 20.0, 21.5, 23.0, and 24.5 wt% relative to PVA, yielding SAFGs with varying degrees of modification. The resulting gel granules were immersed in synthetic Tahe brine (TDS = 2.1 × 10^5 mg/L) and subjected to constant elevated temperatures in a thermostatic chamber. Self-adhesion behavior was observed.

2.8. Thermal stability test

SAFGs were sealed in aging tubes containing either deionized water or synthetic Tahe formation water and thermally aged at elevated temperatures (80–130 °C) for 180 d. The volume retention rate ($R_{vr} = V_{pre\text{-}aging}/V_{post\text{-}aging}$) of samples aged at 130 °C was subsequently measured for use in RSM optimization. Finally, the aged granules were visually inspected and mechanically characterized using a universal testing machine.

2.9. Transportation and plugging evaluation

The transportation and plugging performance of the SAFGs was systematically assessed using a fractured-core flooding setup (Fig. 1). Initially, the selected SAFG formulation was dispersed in an HPAM solution (5000 mg/L) to form a uniform suspension. The fractured core model, prepared with predefined apertures (e.g., 0.1–2.0 mm), was placed into the core holder under a confining pressure of 2.0 MPa. After establishing a stable baseline with HPAM injection, the SAFG suspension was injected at a specified flow rate (typically 2 mL/min) until the differential pressure across the core stabilized. The injection was followed by a second HPAM flood to observe the post-plugging pressure response. Throughout the process, key variables, including granule size, fracture width, injection rate, and SAFG concentration, were varied to characterize the migration patterns and

Table 2
Proportion of scoring responses and scoring rules.

Response	Yield, %	Swelling degree	Thermal stability	Mechanical property
Score	30	20	30	20
Limit	>50	Each >3	>60	>0.5
Scoring rule	Yield × 0.3	$ESR_w + ESR_s$[a]	$R_{vr} \times 0.3$	$(1-K_c) \times 20$

[a] ESR_w and ESR_s are the equilibrium swelling ratio of SAFGs in DI water and synthetic brine, respectively.

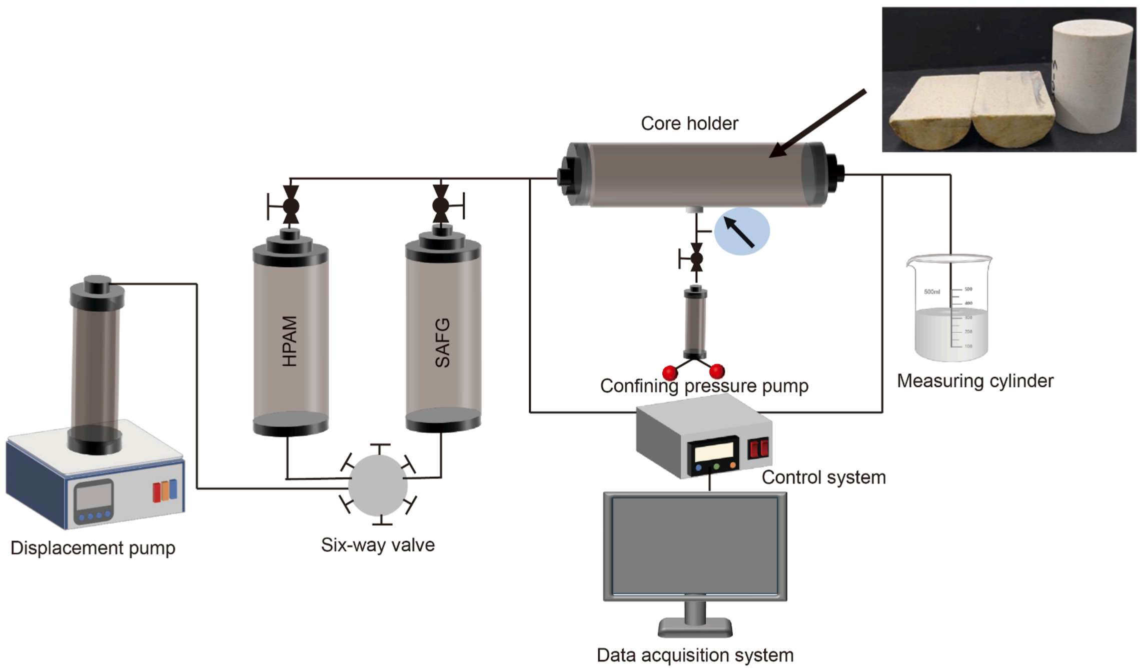

Fig. 1. Simplified schematic diagram of the setup for core flooding experiments.

plugging efficiency of the conformance-control agent. The distribution of retained SAFGs across the inlet, outlet, and longitudinal sections of the fractured core was examined after each test to correlate flow behavior with physical placement.

To evaluate the plugging strength of SAFGs after thermally assisted adhesion, a separate breakthrough pressure test was conducted. After the initial SAFG placement and pressure stabilization, the core holder was sealed and aged at 130 °C for 48 h in high-salinity brine (2.1×10^5 mg/L) to allow for granule adhesion and bulk-gel formation. Following aging, the core was reinstalled in the flooding apparatus. Polymer solution was injected at a constant rate until pressure stabilized. The pump was then switched to constant-pressure mode, and the pressure was incrementally increased (e.g., in 500 kPa steps) until fluid breakthrough occurred. The maximum pressure sustained before breakthrough was recorded as the breakthrough pressure, providing a direct measure of the cohesive strength and plugging stability of the adhered SAFG structure under simulated reservoir conditions.

3. Results and discussion

3.1. Formation of self-adhesive flexible granule (SAFG)

The SAFG system is constructed using PVA as the backbone network, consisting of a hydrophobic (CH_2–CH_2) main chain and hydrophilic (–OH) side groups. Direct cross-linking of PVA with terephthalaldehyde typically yields a bulk gel. To achieve granule formation in an aqueous phase, a hydrophobic modification strategy is first applied to the hydrophilic hydroxyl groups of PVA. This introduces hydrophobic segments, leading to the formation of metastable gel granules through hydrophobic association and phase separation (Fig. 2). While this step creates initial granular structures, they lack long-term stability. Therefore, a subsequent chemical cross-linking step with TAD is employed, consuming part of the remaining hydroxyl groups to form stable acetal linkages and transforming the metastable assemblies into robust and performance-optimized self-adhesion flexible granules. FT-IR analysis confirms the chemical modifications (Fig. S2), evidenced by the characteristic C–O–C stretching vibration at around 1100 cm^{-1} and the presence of aromatic ring vibrations, which verify successful incorporation of the hydrophobic modifier and formation of the intended covalent bonds.

SEM analysis reveals the distinct morphological evolution and enhanced stability achieved through the synthesis process, as shown in Fig. 3. SEM images shown in (Fig. 3(a) and (b)) depict the microstructure of PVA after only the initial hydrophobic modification. In contrast to the smooth, non-porous structure formed by the hydrophobically modified material alone, SEM images shown in Fig. 3(c) and (d) show the morphology of the final SAFGs after complete hydrophobic modification and chemical cross-linking. The granules exhibit a denser, more cohesive structure with a compact, porous internal morphology. This dense yet porous architecture is critical for the performance of granules, enhancing their water absorption capacity while simultaneously allowing efficient energy dissipation under stress, thereby improving mechanical properties. The stability of this optimized structure is

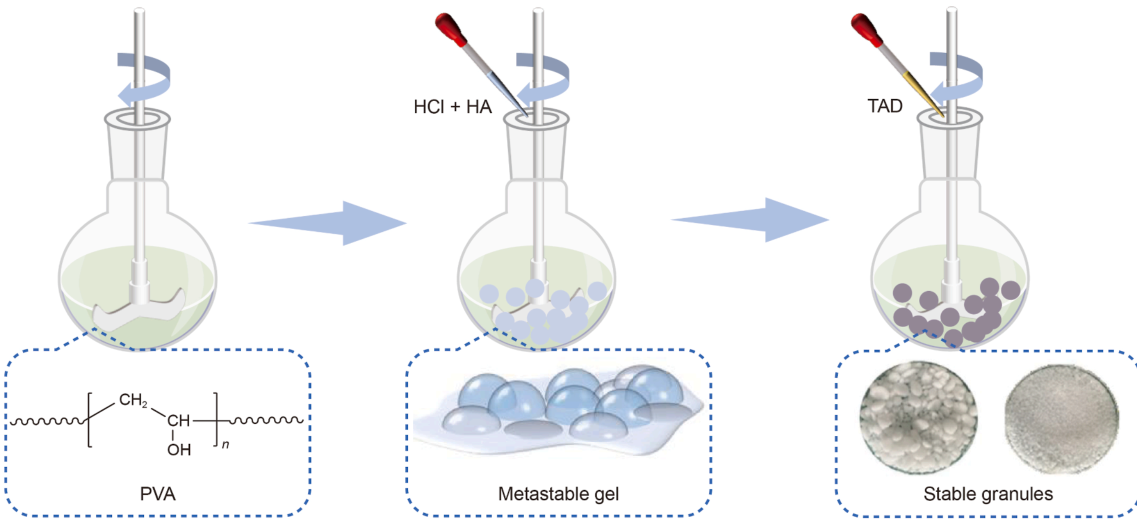

Fig. 2. Schematic diagram of the formation of self-adhesive flexible granules (SAFGs).

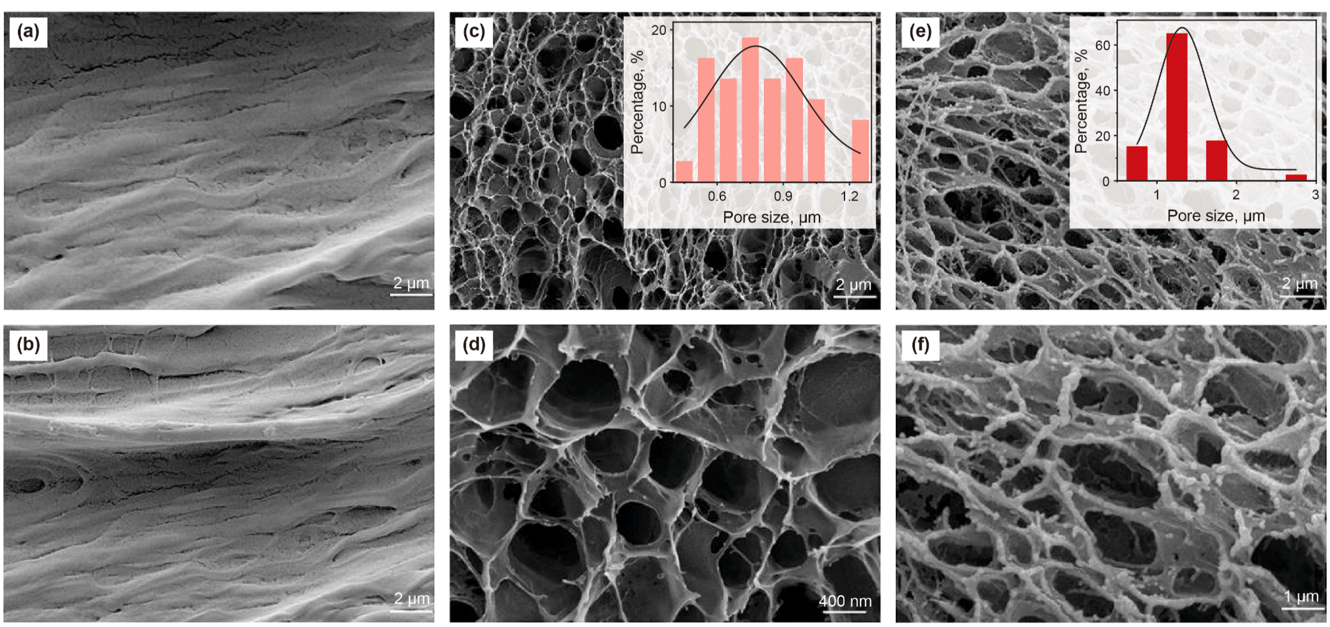

Fig. 3. SEM images of hydrophobically modified PVA (**a**, **b**), SAFGs (**c**, **d**), and the aged SAFGs (**e**, **f**). The inserted bar charts in (c) and (e) show the pore size distribution of SAFGs before and after aging, respectively.

rigorously tested. SEM images shown in (Fig. 3(e) and (f)) present SAFGs after aging for 180 d under extreme conditions of high salinity (2.1×10^5 mg/L) and high temperature (130 °C). Quantitative pore-size analysis shows that, after aging, small pores (~0.6 μm) partially disappear, with pores concentrating around 1 μm, likely due to pore coalescence, while the overall porous structure remains stable. Remarkably, the granules maintain their structural integrity without significant degradation or collapse, demonstrating exceptional long-term thermal and saline stability for applications in harsh reservoir environments.

3.2. Effect of stirring speed on granule size

The stirring speed directly governs the granule size distribution of SAFGs by controlling shear intensity and dispersion. Experimental results (Fig. 4) show that increasing the speed from 280 to 370 rpm significantly reduces granule size, shifting over 80 wt% of the granules from above 3.4 mm to below 0.8 mm. This demonstrates that higher stirring speeds enhance reactant dispersion and phase separation, thereby promoting the formation of smaller, more uniform granules.

Based on this relationship, the stirring speed can be precisely adjusted during synthesis to tailor the granule size according to specific fracture or pore-throat dimensions in target reservoirs. A recommended range of 300–350 rpm yields particles between 0.4 and 2.0 mm in diameter, suitable for conformance control in fractured formations. This controllability enables optimized plugging performance and efficient fluid diversion in heterogeneous reservoirs.

3.3. Analysis of response surface models

3.3.1. Optimization of synthesis process using RSM

A Box–Behnken experimental design was employed to investigate the effects of key process parameters, including stirring

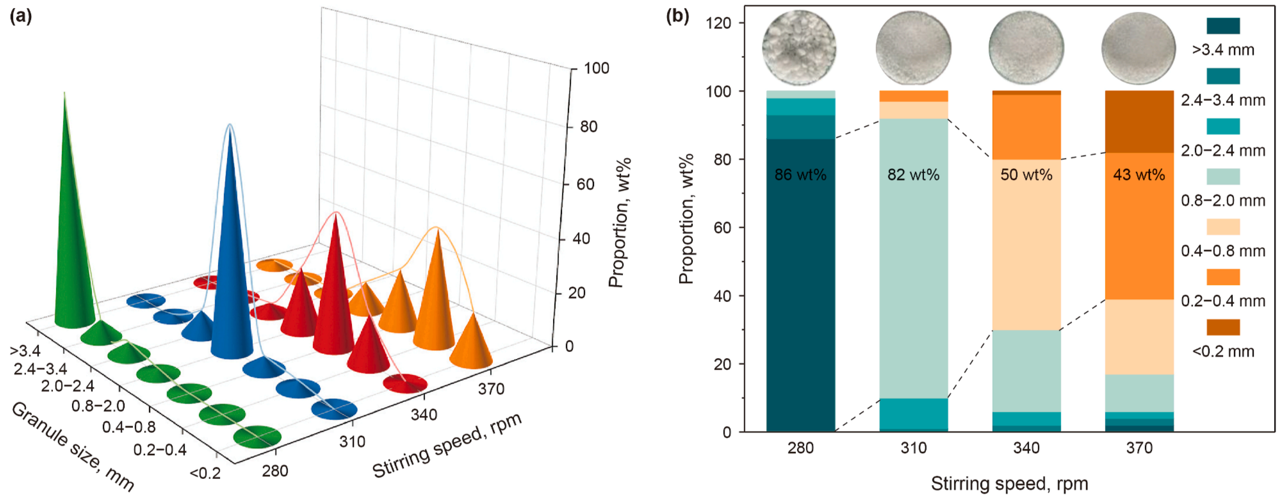

Fig. 4. (**a**) Evolution of granule size distribution of SAFGs with increasing stirring speed (m(HA/PVA) = 21.5 wt%, c(PVA) = 7.5 wt%). (**b**) Corresponding variations in granule composition and the proportion of granules in the dominant sizes.

speed, hydrophobic modifier content, and PVA concentration, on the comprehensive performance score of the synthesized SAFGs. Based on the experimental data, a quadratic polynomial regression model was established to describe the relationship between these independent variables and the response. The final regression equation and the detail of variance analysis are presented as Eq. (2) and Table 3 (Table S2), respectively.

$$Y = 9.42 + 4.05X_1 + 3.68X_2 + 3.05X_3 - 2.03X_1X_2 - 0.125X_1X_3 - 3.28X_2X_3 - 5.95{X_1}^2 - 6.75{X_2}^2 - 7.95{X_3}^2 \quad (2)$$

As the variance analysis of regression model shows (Table S3), the model exhibited a highly significant F-value of 49.72 with a corresponding p-value of less than 0.0001, confirming its statistical significance. The non-significant lack-of-fit term ($p = 0.3828$) further validated the adequacy of the chosen quadratic model. Analysis of individual model terms revealed that the linear effects of all three factors, the interaction effects between X_1 and X_2 (X_1X_2) and X_2 and X_3 (X_2X_3), and all quadratic terms (X_1^2, X_2^2, X_3^2) were statistically significant ($p < 0.05$) (Simsek and Uslu, 2020). The interaction term X_1X_3 was not significant. The order of factor significance, determined by the magnitude of the F-values, was stirring speed (X_1) > hydrophobic modifier content (X_2) > PVA concentration (X_3).

Table 3
Experimental results of RSM.

No.	Stirring speed, rpm	m(HA/PVA), wt%	c(PVA), wt%	Score
1	340	23.0	9.0	59.3
2	310	20.0	7.5	46.9
3	340	21.5	7.5	69.3
4	340	21.5	7.5	69.6
5	310	21.5	9.0	54.7
6	340	23.0	6.0	58.6
7	340	20.0	6.0	43.6
8	340	21.5	7.5	70.1
9	340	20.0	9.0	57.4
10	370	21.5	9.0	61.3
11	370	21.5	6.0	56.6
12	370	20.0	7.5	60.3
13	370	23.0	7.5	62.5
14	340	21.5	7.5	69.4
15	340	21.5	7.5	71.1
16	310	21.5	6.0	49.5
17	310	23.0	7.5	57.2

Model reliability was assessed by analyzing the residuals and the correlation between predicted and experimental values (Fig. S3). The residuals followed a normal distribution, indicating no systematic error. A high coefficient of determination ($R^2 = 0.9845$) demonstrated an excellent fit, with predicted values closely aligning with the actual experimental data. These results collectively confirm the robustness and predictive capability of the developed RSM model for optimizing the SAFG synthesis process.

3.3.2. *Analysis of interaction effects via RSM*

The interaction effects between the process variables on the comprehensive score were visualized and analyzed using three-dimensional response surface plots and their corresponding contour plots.

Based on the response surface analysis, the comprehensive score initially increases with higher stirring speed and HA content, primarily due to improved mixing efficiency and enhanced granule stability from hydrophobic interactions (Figs. 5(a) and S4). However, beyond optimal thresholds, further increases are ineffective or detrimental. Excessive speed generates fine powder particles, while surplus HM offers no additional benefit, indicating effect saturation. When HA content is fixed, PVA concentration shows a parabolic relationship with the score. Moderate PVA aids stabilization, but excess amounts cause agglomeration and reduce modification efficiency (Figs. 5(b) and S5). Lower PVA content improves molecular mobility, favoring hydrophobic modification and particle formation. An inverse correlation exists between optimal PVA and HA contents. Increasing HA within an optimal range improves the score while reducing the required PVA, as HA takes on a greater stabilizing role (Figs. 5(c) and S6). Beyond this range, excessive hydrophobicity weakens hydrogen bonding, impairing granule performance.

The three sets of interactions reveal a synergistic process system where stirring speed acts as a key intensification parameter, reducing reliance on chemical additives. The overall optimum is defined by a balanced triad: sufficient stirring to maximize modifier efficiency, a correspondingly reduced modifier ratio, and a PVA concentration compatible with the chosen shear environment. This interdependence underscores why multivariable RSM

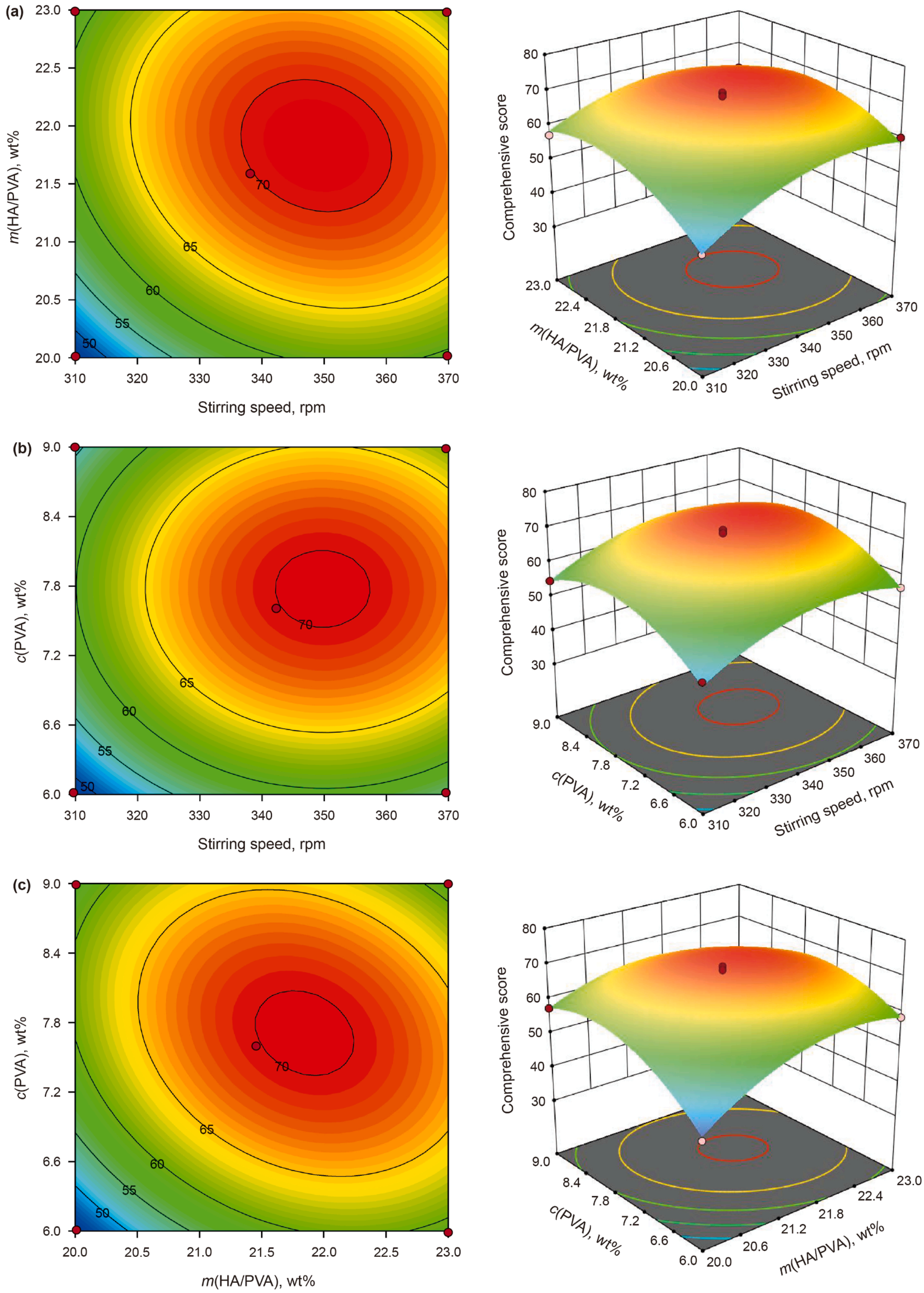

Fig. 5. (**a**) RSM analysis of interaction effect of stirring speed (X_1) and hydrophobic modifier content (X_2) on the comprehensive score at a fixed PVA concentration of 7.5 wt%. (**b**) RSM analysis of interaction effect of stirring speed (X_1) and PVA concentration (X_3) on the comprehensive score with a fixed HA/PVA mass ratio of 21.5 wt%. (**c**) RSM analysis of interaction effect of hydrophobic modifier content (X_2) and PVA concentration (X_3) on the comprehensive score with a stirring speed of 340 rpm. Left: contour image. Right: 3D surface image.

optimization is essential, as single-factor approaches could easily miss this integrated operational window.

3.3.3. Determination and validation of optimal process conditions

Utilizing the established regression model and the desirability function approach within the Design-Expert software, the theoretical optimal process parameters for maximizing the comprehensive score were determined as follows: stirring speed of 349.19 rpm, hydrophobic modifier content of 21.79 wt%, and PVA concentration of 7.73 wt%. This combination yielded a predicted maximum comprehensive score of 71.62. Considering practical feasibility in a laboratory setting, the parameters were slightly adjusted to: stirring speed of 340 rpm, hydrophobic modifier content of 21.5 wt%, and PVA concentration of 7.5 wt%. To validate the model's predictive accuracy, three parallel verification experiments were conducted under these adjusted conditions. The average experimental comprehensive score obtained was 70.2, which is in excellent agreement with the predicted value, exhibiting a deviation of less than 1%. This close correspondence between the predicted and experimental results confirms the accuracy of the RSM model and demonstrates that the identified optimal formulation successfully produces SAFGs with superior comprehensive performance.

3.4. Self-adhesion behavior of SAFGs

The self-adhesion behavior of SAFGs with varying modification degrees was systematically investigated across temperatures from 80 to 130 °C in high-salinity brine. As illustrated in Fig. 6, a distinct correlation exists between the modification degree and the onset temperature required for effective granule adhesion. Specifically, granules with a modification degree of 20.0% initiated adhesion at 90 °C, whereas higher modification levels required correspondingly elevated temperatures: 21.5% at 100 °C, 23.0% at 110 °C, and 24.5% at 120 °C. Notably, monolithic gel formation was observed at 110, 120, and 130 °C under the respective modification conditions. To further verify the thermally activated nature of this adhesion process, DSC analysis was performed (Fig. 7). The thermograms revealed an endothermic transition with onset temperatures matching the adhesion initiation temperatures observed in the visual bottle tests (e.g., 104.2 °C for 20.0% modification and ~116.7 °C for 23.0% modification). The presence of this specific

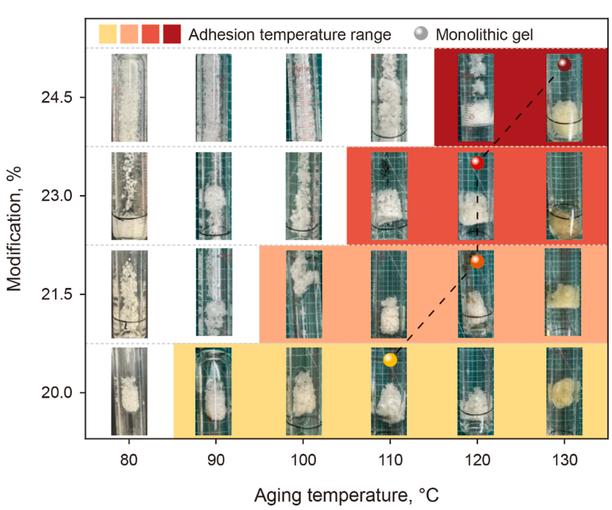

Fig. 6. Self-adhesion behavior of SAFGs as a function of hydrophobic modification degree.

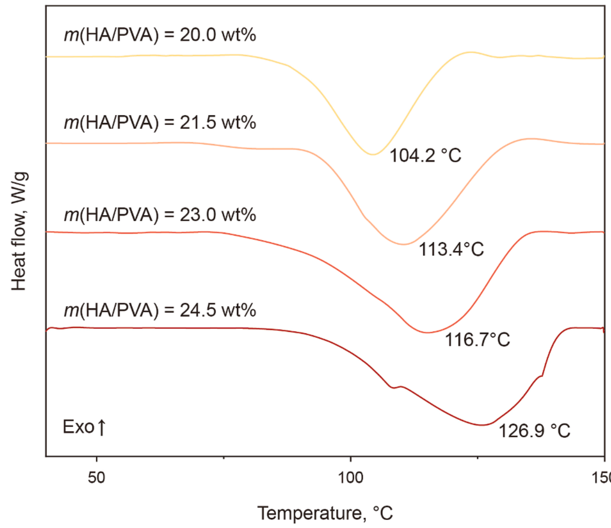

Fig. 7. DSC thermograms of SAFGs with different hydrophobic modification degrees.

endothermic peak confirm that the adhesion is governed by the thermal activation of the SAFG secondary interactions. This trend indicates that the adhesion onset temperature can be precisely tailored by adjusting the modification degree, thereby enabling the customization of SAFG systems for specific reservoir thermal profiles. Such tunability offers significant advantages in field applications, allowing for targeted placement and optimized cost-performance balance in conformance control operations under varying geothermal conditions.

The underlying mechanism of SAFG adhesion is governed by brine-induced intermolecular interactions that are thermally activated (Fig. 8). In contrast to pure aqueous environments, where no adhesion occurs, high-salinity brines containing divalent ions such as Ca^{2+} and Mg^{2+} markedly alter polymer chain behavior. FT-IR analysis of SAFG after high-temperature high-salinity aging revealed a significant red shift of the O–H stretching vibration from ~3340 to ~3321 cm^{-1} with notable peak narrowing and reduced intensity (Fig. S2), confirming the formation of coordination bonds between Ca^{2+} and hydroxyl groups of PVA (Eslamkish et al., 2025; Zhang et al., 2022a). These ions facilitate the formation of coordination bonds and enhance hydrophobic associations among macromolecules, leading to intermolecular linkages that are more robust than those formed solely through hydrogen bonding (Li et al., 2019; Zhao et al., 2015). To confirm that this adhesion is specifically triggered by divalent cations rather than the high concentration of Na^+ present in the simulated brine, we performed a comparison experiment. SAFG granules were independently treated in a high-concentration NaCl solution and a $CaCl_2$ solution at 130 °C. The granules in the $CaCl_2$ solution showed strong inter-granule adhesion after 12 h, whereas those in the NaCl solution remained fully dispersed without any observable adhesion even after 20 h (Table S4). This direct evidence confirms that the divalent ions are the primary drivers of the ion-mediated adhesion mechanism, while Na^+ alone is insufficient to induce the effect. Notably, the increase in modification degree introduces additional hydrophobic moieties into the polymer structure, which raises the energy threshold required for chain interaction and rearrangement (Sarsenbekuly et al., 2017). Consequently, a higher thermal input is necessary to overcome this energy barrier and initiate adhesion, explaining the observed shift in onset temperature with increasing modification level. This ion-mediated interaction not only increases the density of hydrophobic domains

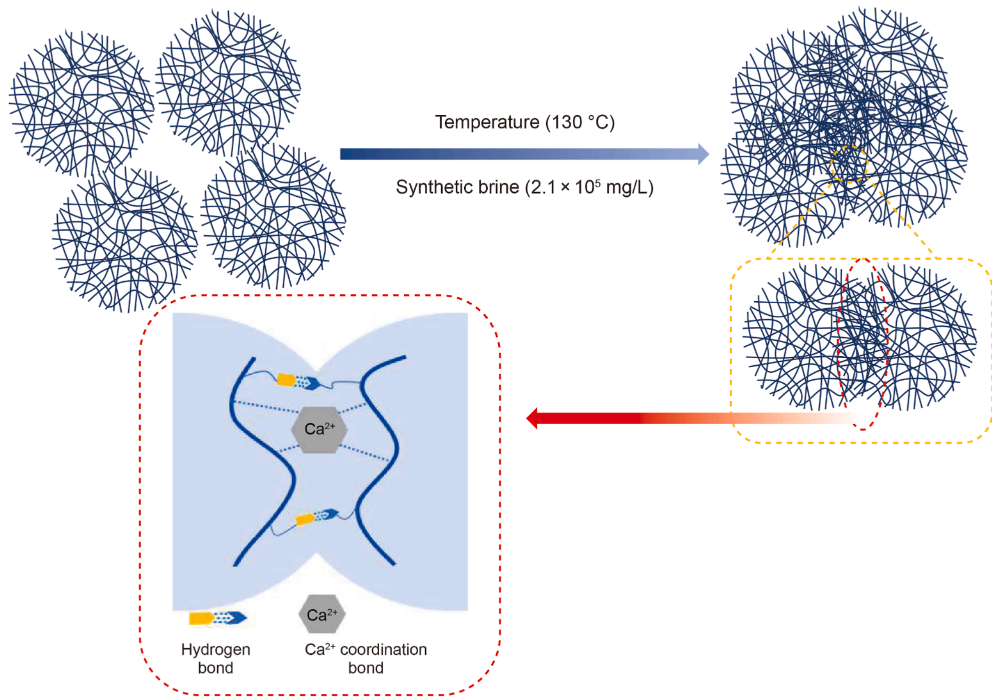

Fig. 8. Schematic illustration of the mechanism of self-adhesion of SAFGs.

but also reinforces the three-dimensional network, thereby promoting effective granule–granule adhesion (Pu et al., 2023; Wang et al., 2023; Zhu et al., 2017).

To further validate this mechanism, a control experiment was conducted using unmodified PVA crosslinked with glutaraldehyde under identical conditions (130 °C, 2.1×10^5 mg/L salinity, 20 d). The unmodified particles remained discrete and non-adhesive (Fig. S7), exhibiting only stiffening due to strong salting-out effects that induce excessive chain collapse. In contrast, the hydrophobic modification in SAFG imparts steric shielding against salt-induced dehydration and acts as an internal plasticizer, preserving chain mobility at elevated temperatures and thereby enabling salt-activated inter-particle adhesion and bulk gel formation. At 130 °C in high-salinity brine, SAFGs undergo extensive adhesion and form cohesive bulk gels capable of conforming to fracture geometries. This salt-activated, thermally assisted adhesion mechanism overcomes the limitations of conventional PPGs, which often exhibit insufficient stability in large flow channels, thereby presenting a reliable strategy for deep-profile water shutoff in fractured, high-temperature, and high-salinity reservoirs.

3.5. *Long-term aging performance of SAFGs under extreme conditions*

To evaluate the long-term stability of SAFGs, the optimal formulation of SAFGs was aged in high-salinity brine at 130 °C inside sealed pressure-resistant tubes. Observations at intervals of 1, 5, 15, 30, 60, 180, and 300 d revealed that the granules began to adhere after one day and progressively formed a cohesive bulk structure over time (Fig. 9). After 300 d of aging, the material maintained its structural integrity with a volume shrinkage rate of only 21.47%, demonstrating exceptional stability under harsh reservoir conditions. Following 180 d of aging, the consolidated bulk remained elastic and exhibited robust mechanical performance. SEM images (Fig. 3(e) and (f)) after 180 d revealed a preserved porous yet dense morphology, corroborating the structural

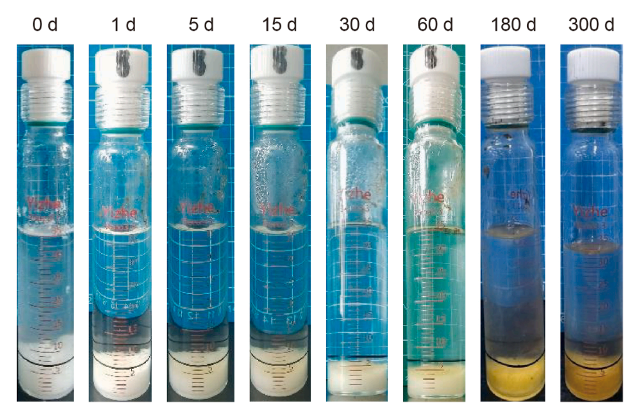

Fig. 9. Aging test results of SAFGs.

resilience imparted by the chemically cross-linked network reinforced with benzene rings. This network effectively resists collapse and retains elasticity under prolonged high-temperature and high-salinity exposure. As shown in Fig. 10, the aged material withstood four consecutive compression cycles under a load of 500 N without significant structural damage, confirming that SAFGs maintain both structural integrity and functional elasticity even after extended high-temperature and high-salinity aging.

The superior aging resistance of SAFGs is fundamentally attributed to enhanced thermal and structural stability resulting from hydrophobic modification and chemical cross-linking. TGA indicates that pure PVA undergoes substantial decomposition through dehydration and backbone cleavage, whereas SAFGs exhibit markedly improved thermal resistance (Fig. S8). Specifically, SAFGs show minimal mass loss between 60 and 250 °C and maintain high stability up to 320 °C. Only above this temperature do side-group elimination and backbone scission become pronounced, leading to network degradation. The improved thermal

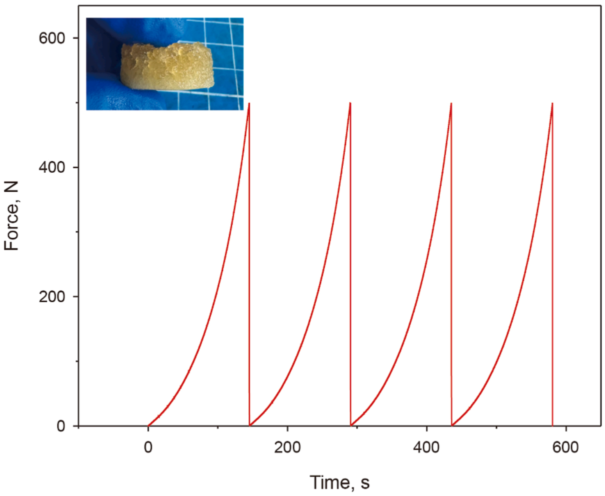

Fig. 10. Cyclic compression response of SAFGs. The inset shows the gel bulk after testing.

stability is largely attributed to the benzene-ring moieties from TAD, which restrict chain mobility and delay thermal degradation, thereby preserving structural integrity under simulated reservoir conditions. This enhanced stability, enabling SAFGs to withstand temperatures exceeding typical reservoir conditions, stems primarily from the reinforced cross-linked network and hydrophobic interactions. In high-salinity brine, hydrophobic domains, combined with ion-mediated coordination, further stabilize the three-dimensional structure by limiting polymer chain mobility and mitigating thermal-oxidative degradation. Consequently, SAFGs not only endure prolonged exposure to ultra-high temperature and salinity but also retain their adhesive capability and mechanical elasticity. These characteristics establish SAFGs as a durable and reliable material for long-term conformance control in demanding high-temperature and high-salinity reservoirs.

3.6. Transportation and plugging performance

Preliminary screening experiments determined the optimal matching relationships between SAFG granule size and fracture

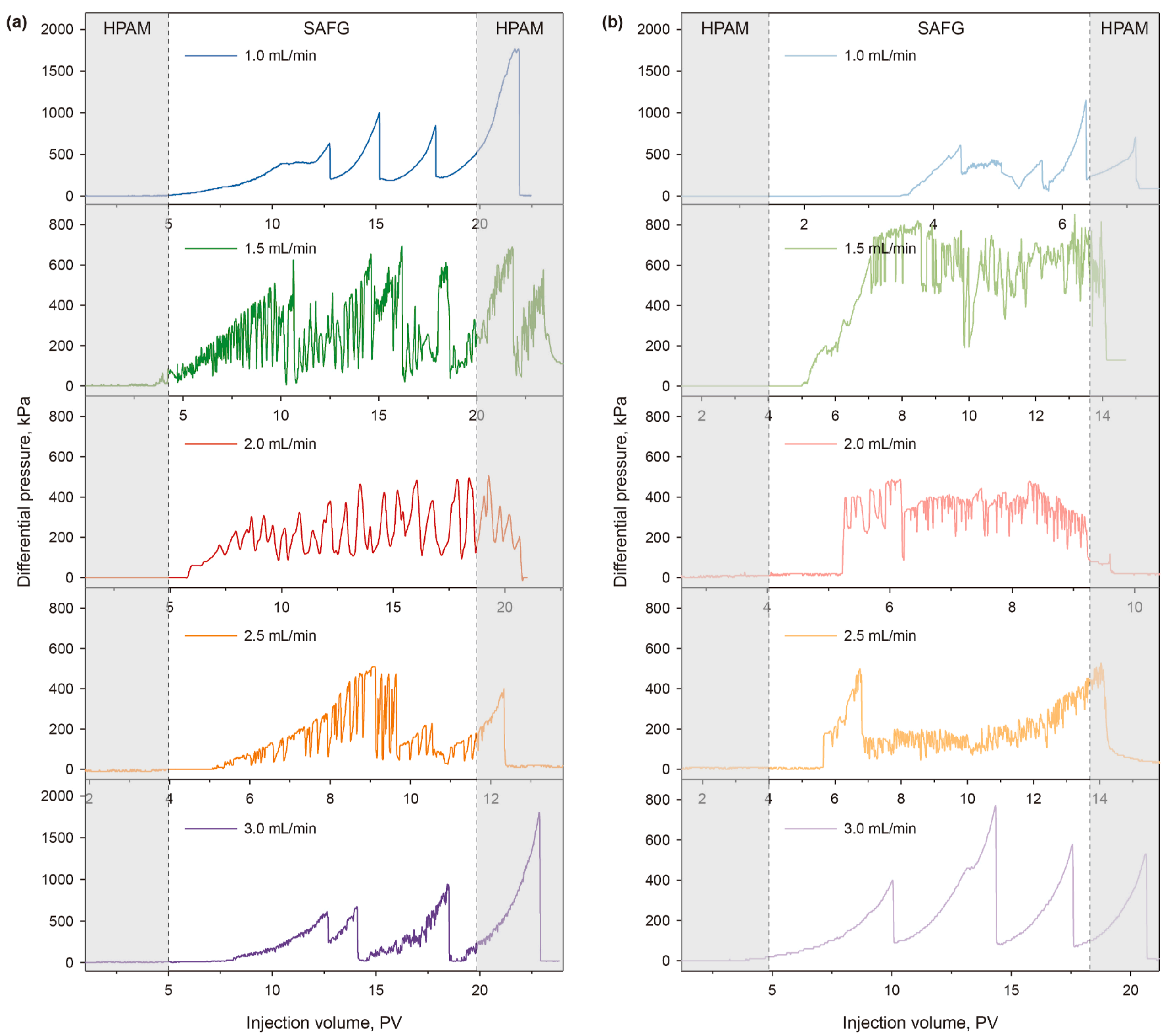

Fig. 11. Differential pressure evolution during SAFGs transport in fractures at varying injection rates. (**a**) For 0.4–0.8 mm granules in 0.5 mm-wide fracture. (**b**) For 0.8–2.0 mm granules in 1.0 mm-wide fracture.

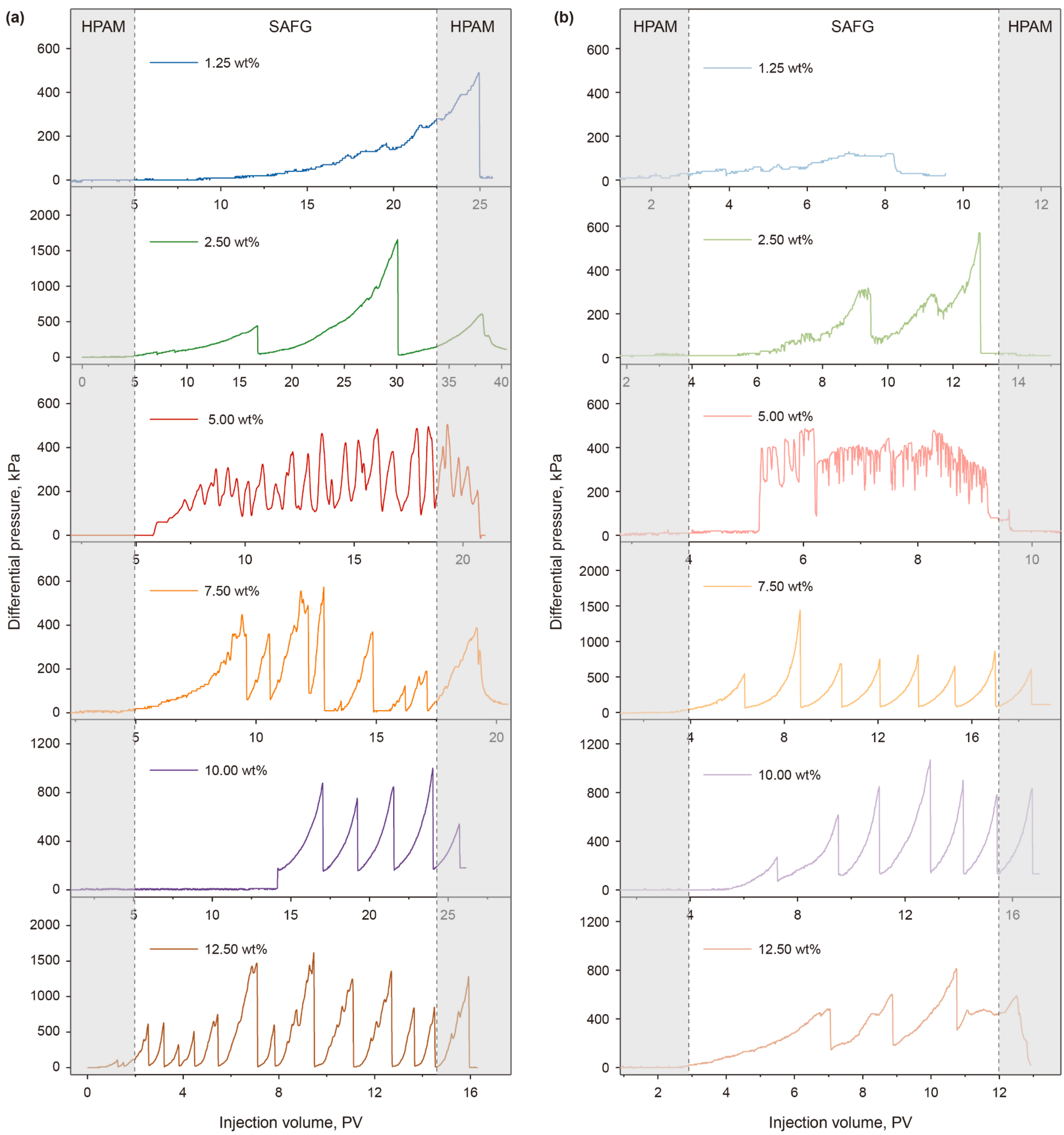

Fig. 12. Differential pressure evolution during SAFGs transport in fractures at varying granule concentrations. (**a**) For 0.4–0.8 mm granules in 0.5 mm-wide fracture. (**b**) For 0.8–2.0 mm granules in 1.0 mm-wide fracture.

width (Fig. S9, Table S5). Subsequently, systematic core flooding tests were conducted to evaluate the influence of injection rate and granule concentration on the migration and plugging behavior of the selected optimal SAFG formulations (20–40 mesh for 0.5 mm-wide fractures and 10–20 mesh for 1.0 mm-wide fractures).

3.6.1. Effect of injection rate on the transportation and plugging performance

The impact of injection rate on differential pressure characteristics was investigated across a range of 1.0 to 3.0 mL/min. As illustrated in Fig. 11 and Table S6, an injection rate of 1.0 mL/min resulted in relatively high and less fluctuating pressure differentials, indicating limited granule migration due to potential accumulation at the fracture entrance. Within the optimal range of 1.5 to 2.5 mL/min, the differential pressure profiles exhibited consistent and frequent fluctuations. This pattern signifies an effective cyclical process of granule bridging, accumulation, deformation, breakthrough, and re-plugging within the fracture, which is crucial for deep fluid diversion. The amplitude of these pressure fluctuations was largely independent of the flow rate within this range, aligning with field observations where injection pressure is often insensitive to rate changes. However, at a higher injection rate of 3.0 mL/min, the differential pressure increased significantly. The

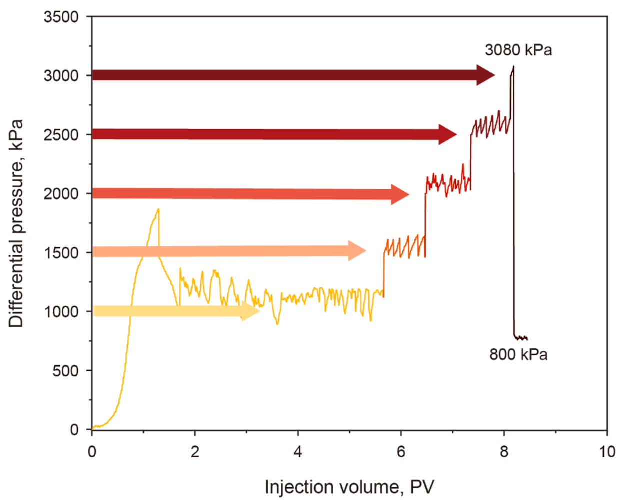

Fig. 13. Breakthrough pressure and steady-state flow differential pressure for fracture treated by self-adhered SAFGs.

excessive hydrodynamic force hindered effective granule bridging, causing premature granule washout through the fracture and thereby reducing plugging stability.

3.6.2. *Effect of granule concentration on the transportation and plugging performance*

The effect of SAFG concentration was studied from 1.25 to 12.50 wt%. As shown in Fig. 12 and Table S7, at lower concentrations (1.25–2.50 wt%), pressure buildup was slow and less pronounced, reflecting the extended time required for sufficient granule accumulation to form an effective plug. At the optimal concentration of 5.00 wt%, the differential pressure curve displayed frequent and regular oscillations, demonstrating excellent migration and dynamic plugging efficiency. This behavior corresponds to the repeated cycle of granule retention, pressure buildup, deformation/breakthrough, and re-accumulation. Higher concentrations (7.50–12.50 wt%) led to a rapid initial pressure increase and more complex fluctuation patterns, as the dense particle slurry accelerated the filling and sealing of the fracture network, though potentially increasing near-wellbore injection pressure.

3.6.3. *Breakthrough pressure test after self-adhesion*

A key performance evaluation involved testing the breakthrough pressure of adhered SAFG blocks. After initial injection and stabilization, the core containing lodged SAFGs was aged to allow for adhesion, forming a cohesive gel block. Subsequent polymer injection into this blocked fracture (Fig. 13) revealed a significantly enhanced plugging strength. The breakthrough pressure for the adhered SAFG reached 3080 kPa, approximately 6.3 times its initial stabilization pressure (~490 kPa), underscoring the strength enhancement via thermally assisted adhesion. After breakthrough, under a constant injection rate of 2.0 mL/min, the systems re-stabilized at a differential pressure of 800 kPa. These results confirm that the adhesion process transforms a mobile particle pack into a robust, coherent gel with substantially increased mechanical strength and plugging integrity, capable of withstanding much higher pressure gradients. This is a critical advantage for long-term conformance control in fractured reservoirs.

4. Conclusions

(1) A novel self-adhesive flexible granule was successfully synthesized through a sequential process of hydrophobic modification and chemical cross-linking of PVA. The synthesis process is controllable, allowing for precise tuning of granule size distribution through adjustment of stirring speed to match target fracture apertures.
(2) The self-adhesion behavior of SAFGs is a thermally activated process specific to high-salinity environments, governed by ion-mediated hydrophobic associations and coordination bonds. The onset temperature for adhesion can be precisely tailored (90–120 °C) by adjusting the degree of hydrophobic modification, enabling customization for specific reservoir thermal profiles.
(3) SAFG demonstrates exceptional long-term stability under extreme reservoir-simulated conditions (130 °C, salinity of 2.1×10^5 mg/L), maintaining structural integrity and mechanical elasticity after 180 d of aging. This stability is attributed to the reinforced network from hydrophobic modification and benzene-ring cross-linking.
(4) Core-flooding evaluations reveal that SAFG exhibits effective migration and dynamic plugging in fractures, characterized by cyclical bridging, deformation, and re-plugging. The optimal injection performance was achieved at rates of 1.5–2.5 mL/min and a granule concentration of 5.00 wt%.
(5) The thermally assisted adhesion process transforms injected SAFG granules into a coherent, bulk gel structure within the fracture, resulting in a significant enhancement of plugging strength. The adhered SAFG achieved a breakthrough pressure of 3080 kPa, confirming its superior potential for forming durable seals and enabling deep fluid diversion in high-temperature and high-salinity fractured reservoirs.

CRediT authorship contribution statement

Yan Xue: Writing – original draft, Validation, Project administration, Methodology, Formal analysis, Conceptualization. **Xiao-Feng Zhao:** Validation, Investigation, Data curation. **Qiu-Lu Yin:** Investigation, Data curation. **Jing-Yang Gu:** Validation, Data curation. **Bing Wei:** Writing – review & editing, Supervision, Funding acquisition. **Jun Lu:** Writing – review & editing, Resources, Funding acquisition.

Declaration of competing interest

The authors declare that they have no known competing financial interests or personal relationships that could have appeared to influence the work reported in this paper.

Acknowledgments

The authors gratefully acknowledge the financial support from the National Natural Science Foundation of China (52274041). Jun Lu acknowledges the McDougall School of Petroleum Engineering at The University of Tulsa for the support of this research. The authors also sincerely appreciate the anonymous reviewers for their valuable comments.

Appendix A. Supplementary data

Supplementary data to this article can be found online at https://doi.org/10.1016/j.petsci.2026.06.019.

References

Al Brahim, A., Eriyagama, Y., Bai, B., et al., 2023. Feasibility study of recrosslinkable preformed particle gels for natural gas injection profile control. SPE J. 28 (4), 1829–1841. https://doi.org/10.2118/210127-PA.

Alotibi, A., Song, T., Bai, B., et al., 2025. Transport and plugging performance evaluation of a novel recrosslinkable microgel used for conformance control in mature oil fields with superpermeable channels. SPE J. 30 (2), 823–835. https://doi.org/10.2118/215168-PA.

Auta, M., Hameed, B.H., 2011. Optimized waste tea activated carbon for adsorption of methylene blue and acid blue 29 dyes using response surface methodology. Chem. Eng. J. 175, 233–243. https://doi.org/10.1016/j.cej.2011.09.100.

Bai, B., Zhou, J., Yin, M., 2015. A comprehensive review of polyacrylamide polymer gels for conformance control. Petrol. Explor. Dev. 42 (4), 525–532. https://doi.org/10.1016/s1876-3804(15)30045-8.

Bu, Y., Wang, G., Ren, M., et al., 2024. Development of a plugging material featuring external flexibility and internal rigidity. Colloids Surf., A 697, 134294. https://doi.org/10.1016/j.colsurfa.2024.134294.

Eslamkish, F., Nazari, A., Mohammadi, M.H., et al., 2025. Reinforcement of polyvinyl alcohol hydrogels with calcium ions and iron oxide nanoparticles: Effects on morphology, swelling, and mechanical properties. Results Eng. 28, 107582. https://doi.org/10.1016/j.rineng.2025.107582.

Gao, Y., Cheng, H., Li, G., et al., 2026. Gelation and reservoir conformance control performance of in situ crosslinked polymer gels prepared with different crosslinkers. Pet. Sci. 23 (4), 2075–2085. https://doi.org/10.1016/j.petsci.2026.01.003.

Kumar, A., Mahto, V., Sharma, V.P., 2020. Reinforced preformed particle gel: Synthesis, characterization and performance evaluation for water shut-off jobs in heterogeneous reservoir. J. Pet. Sci. Eng. 193, 107408. https://doi.org/10.1016/j.petrol.2020.107408.

Leng, J., Wei, M., Bai, B., 2021. Review of transport mechanisms and numerical simulation studies of preformed particle gel for conformance control. J. Pet. Sci. Eng. 206, 109051. https://doi.org/10.1016/j.petrol.2021.109051.

Li, X., Yin, H., Zhang, R., et al., 2019. A salt-induced viscosifying smart polymer for fracturing inter-salt shale oil reservoirs. Pet. Sci. 16 (4), 816–829. https://doi.org/10.1007/s12182-019-0329-3.

Mehrabianfar, P., Malmir, P., Soulgani, B.S., et al., 2020. Study on the optimization of the performance of preformed particle gel (PPG) on the isolation of high permeable zone. J. Pet. Sci. Eng. 195, 107530. https://doi.org/10.1016/j.petrol.2020.107530.

Pu, J., Bai, B., Alhuraishawy, A., Schuman, T., Chen, Y., Sun, X., 2019. A recrosslinkable preformed particle gel for conformance control in heterogeneous reservoirs containing linear-flow features. SPE J 1714–1725.

Pu, J., Bai, B., Geng, J., et al., 2023. Dual crosslinked poly(acrylamide-co-N-vinylpyrrolidone) microspheres with re-crosslinking ability for fossil energy recovery. Geoenergy Sci. Eng. 224, 211604. https://doi.org/10.1016/j.geoen.2023.211604.

Qiu, Y., Wei, M., Bai, B., 2017. Descriptive statistical analysis for the PPG field applications in China: Screening guidelines, design considerations, and performances. J. Pet. Sci. Eng. 153, 1–11. https://doi.org/10.1016/j.petrol.2017.03.030.

Salunkhe, B., Schuman, T., Al Brahim, A., et al., 2021. Ultra-high temperature resistant preformed particle gels for enhanced oil recovery. Chem. Eng. J. 426, 130712. https://doi.org/10.1016/j.cej.2021.130712.

Sarsenbekuly, B., Kang, W., Fan, H., et al., 2017. Study of salt tolerance and temperature resistance of a hydrophobically modified polyacrylamide based novel functional polymer for EOR. Colloids Surf., A 514, 91–97. https://doi.org/10.1016/j.colsurfa.2016.10.051.

Schuman, T., Salunkhe, B., Al Brahim, A., et al., 2022. Evaluation of ultrahigh-temperature-resistant preformed particle gels for conformance control in north sea reservoirs. SPE J. 27 (6), 3660–3673. https://doi.org/10.2118/206007-PA.

Seidy Esfahlan, M., Khodapanah, E., Tabatabaei-Nezhad, S.A., 2021. Comprehensive review on the research and field application of preformed particle gel conformance control technology. J. Pet. Sci. Eng. 202, 108440. https://doi.org/10.1016/j.petrol.2021.108440.

Seright, R., Brattekas, B., 2021. Water shutoff and conformance improvement: An introduction. Pet. Sci. 18 (2), 450–478. https://doi.org/10.1007/s12182-021-00546-1.

Simsek, S., Uslu, S., 2020. Determination of a diesel engine operating parameters powered with canola, safflower and waste vegetable oil based biodiesel combination using response surface methodology (RSM). Fuel 270, 117496. https://doi.org/10.1016/j.fuel.2020.117496.

Song, T., Ahdaya, M., Zhao, S., et al., 2022. Evaluation of a novel recrosslinkable hyperbranched preformed particle gel for the conformance control of high-temperature reservoirs with fractures. SPE J. 27 (6), 3598–3610. https://doi.org/10.2118/209451-PA.

Sun, L., Li, D., Pu, W., et al., 2020. Combining preformed particle gel and curable resin-coated particles to control water production from high-temperature and high-salinity fractured producers. SPE J. 25 (2), 938–950. https://doi.org/10.2118/198887-PA.

Tak, B.Y., Tak, B.S., Kim, Y.J., et al., 2015. Optimization of color and cod removal from livestock wastewater by electrocoagulation process: Application of box–behnken design (BBD). J. Ind. Eng. Chem. 28, 307–315. https://doi.org/10.1016/j.jiec.2015.03.008.

Wang, L., Long, Y., Ding, H., et al., 2017. Mechanically robust re-crosslinkable polymeric hydrogels for water management of void space conduits containing reservoirs. Chem. Eng. J. 317, 952–960. https://doi.org/10.1016/j.cej.2017.02.140.

Wang, R., Wang, C., Long, Y., et al., 2023. Preparation and investigation of self-healing gel for mitigating circulation loss. Adv. Geo-Energy Res. 8 (2), 112–125. https://doi.org/10.46690/ager.2023.05.05.

Wang, Z., Bai, B., 2018. Preformed-particle-gel placement and plugging performance in fractures with tips. SPE J. 23 (6), 2316–2326. https://doi.org/10.2118/193997-PA.

Wu, R., Wei, B., Li, S., et al., 2023. Enhanced oil recovery in complex reservoirs: Challenges and methods. Adv. Geo-Energy Res. 10 (3), 208–212. https://doi.org/10.46690/ager.2023.12.07.

Wu, W., Hou, J., Qu, M., et al., 2022. A novel polymer gel with high-temperature and high-salinity resistance for conformance control in carbonate reservoirs. Pet. Sci. 19 (6), 3159–3170. https://doi.org/10.1016/j.petsci.2022.05.003.

Xue, Y., Yin, Q., Zhang, C., et al., 2024. Self-granulating thermoplastic elastic particles for fracture conformance control in ultraharsh reservoirs: Laboratory investigation and field application. SPE J. 29 (12), 7134–7147. https://doi.org/10.2118/218155-PA.

Zhai, Y., Fang, Z., Feng, J., et al., 2024. Development and performance evaluation of recrosslinkable preformed particle gel under high temperature and high salt conditions. Polymer 296, 126824. https://doi.org/10.1016/j.polymer.2024.126824.

Zhang, S., Wan, Y., Yuan, W., et al., 2022a. Preparation of PVA-CS/SA-Ca^{2+} hydrogel with core-shell structure. Polymers 14 (1), 212. https://doi.org/10.3390/polym14010212.

Zhang, X., Deng, J., Yang, K., et al., 2022b. High-strength and self-degradable sodium alginate/polyacrylamide preformed particle gels for conformance control to enhance oil recovery. Pet. Sci. 19 (6), 3149–3158. https://doi.org/10.1016/j.petsci.2022.06.012.

Zhao, S., Al Brahim, A., Liu, J., et al., 2022. Coreflooding evaluation of fiber-assisted recrosslinkable preformed particle gel using an open fracture model. SPE J. 28 (1), 268–278. https://doi.org/10.2118/212282-pa.

Zhao, T., Xing, J., Dong, Z., et al., 2015. Synthesis of polyacrylamide with superb salt-thickening performance. Ind. Eng. Chem. Res. 54 (43), 10568–10574. https://doi.org/10.1021/acs.iecr.5b02718.

Zhu, Z., Kang, W., Yang, H., et al., 2017. Study on salt thickening mechanism of the amphiphilic polymer with betaine zwitterionic group by β-cyclodextrin inclusion method. Colloid Polym. Sci. 295 (10), 1887–1895. https://doi.org/10.1007/s00396-017-4169-7.